ELSEVIER

Precision Engineering 23 (1999) 51–62

PRECISION ENGINEERING

Examination of surface location error due to phasing of cutter vibrations

Tony Schmitz *, John Ziegert

Machine Tool Research Center, Department of Mechanical Engineering, 237 MEB, University of Florida, Gainesville, FL 32611 USA

Manuscript received 8 April 1998; revised 31 August 1998; accepted 24 September 1998

Abstract

The purpose of this research is to investigate the relative importance of spindle speed, system dynamics, and cutting conditions on the accuracy of surface location in computer numerical-control (CNC) finish machining operations. The relationship between the spindle speed, the most flexible modes of the machine/cutting tool system and the final part dimensions is rather complex. The underlying theory, based on the situation of forced vibrations, is outlined. It is shown that the critical factor is the ratio of the tooth passing frequency to the system most flexible mode and corresponding natural frequency. Simple analytical calculations are carried out to illustrate the overcut/undercut surface error phenomenon. A simple simulation for end milling operations is also described which calculates the force on the cutter, the resulting cutter deflection, and the final error of surface. A comparison between the simulated and experimental results is presented. From experimental data, it shown that a change in surface location (and part dimension) of up to 50 μm is seen for a set of given conditions (i.e., cutter, material, chip load) simply by changing spindle speeds. Furthermore, it is seen that certain spindle speeds produce surfaces with no error introduced by the machining process.

1. Introduction

In computer numerical-control (CNC) machining, accurate positioning of the tool with respect to the workpiece for material removal is required. The machine tool's performance can be evaluated by the machine's contouring accuracy, cutting performance, and/or repeatability [1]. Sources which cause errors in these categories are geometric and thermal errors, typically termed quasi-static errors, imperfect spindle motions, friction in the drives, controller errors and cutting force errors. To reduce the errors in the machining process, the techniques of avoidance and/or error compensation may be used [2]. In avoidance, design procedures and high quality components are employed to remove the source(s) of the errors. In compensation, the effect of the error is removed, although the actual error source remains. Compensation, normally implemented in software, uses "pre-process data, a machine model, and indirect sensing of process parameters" to correct the errors in real time [3]. A typical example of software compensation is reversal compensation, which nearly all commercial machine tools utilize. To correct for the reversal error, encoder counts are injected or suppressed by the controller after a reversal of motion to remove this common positioning error.

The purpose of this research is to investigate the relative importance of spindle speed, system dynamics, and cutting conditions on the accuracy of surface location in CNC finish machining operations. The cutter deflections, which produce the surface location errors investigated here, are not easily adaptable to real-time compensation. However, as will be shown, proper selection of spindle speed in the NC program may increase the surface location accuracy and act as a type of "NC avoidance."

2. Forced vibrations and surface location error

The relationship between the spindle speed, the most flexible modes of the machine/cutting tool system, and the final part dimensions is not a simple one. It has been discussed in literature by Tlusty [4], Smith [5], and Altintas [6] and will be detailed in the following paragraphs.

As shown in Fig. 1, cutter deflections during end milling will only affect the final surface when a tooth is in position 1. In up milling (Fig. 1a), the error of location is defined as the displacement of the cutter relative to the commanded depth of cut when a tooth enters the cut. In down milling, the

* Corresponding author. Tel: (352) 392-7573; Fax: (352) 392-1071; E-mail: tony26@grove.ufl.edu.

0141-6359/99/$–see front matter
PII: S0141-6359(98)00025-7

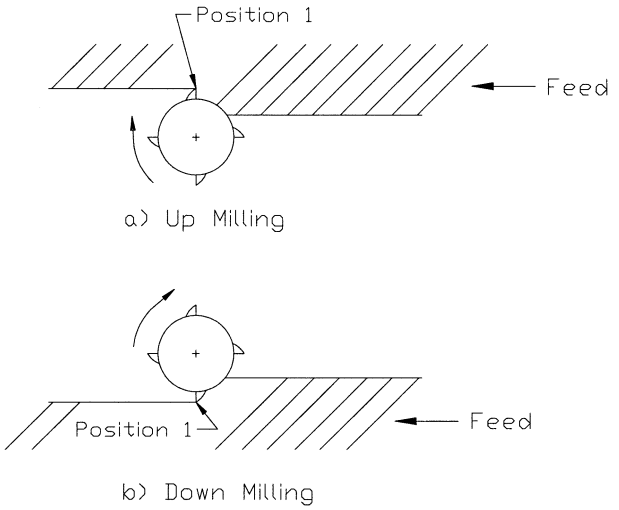

Fig. 1. Up/down milling.

error is defined as the cutter displacement relative to the desired surface when a tooth disengages from the cut [7]. At other angular orientations of the tool, any imprint of the cutter deflection on the material will be removed by succeeding teeth.

As the cutter impacts the workpiece surface, a situation of forced vibration arises in which the dominant forcing frequency is equal to the tooth passing frequency of the cutter, f_{tooth} (see [Eq. 1]). For simple systems under forced vibration, the deflection varies at the same frequency as the force, but lags it in time. The cutting forces are strongly harmonic and cause deflections of the cutter. The amplitude and phase of these deflections depends not only on the system flexibility and cutting conditions, but also on the system natural frequency (i.e., when the forcing frequency is equal to the natural frequency, resonance is observed and large deflections can occur). The crucial factors, therefore, are the spindle speed (proportional to the tooth passing frequency) and the frequency response of the system. As the tooth passing frequency is varied, the magnitude and phase of the cutter vibration change. This, in turn, varies the final surface location.

$$f_{tooth} = nm \ (Hz), \tag{1}$$

where n = spindle speed in rev/s
m = number of teeth on cutting tool.

It is the occurrence of resonance and the importance of the ratio, r, of the forcing frequency to the natural frequency ($r = f_{tooth}/f_n$) that makes this work especially relevant to the field of high-speed machining (HSM). One popular definition of HSM is operation at spindle speeds where the tooth passing frequency can approach a substantial fraction of the system's most flexible natural frequency [8]. Machining at these speeds can dramatically increase the allowable depth of cut for stable machining. By increasing the stable depth of cut, the material removal rate (MRR) can be increased and the machining time substantially reduced [9]. However, operating at these spindle speeds may also adversely affect the workpiece accuracy depending on the tool flexibility (Eq. 2).

$$MRR = b * a * f \ (mm^3/min), \tag{2}$$

where b = axial depth of cut (mm)
a = radial depth of cut (mm)
f = linear feedrate (mm/min).

Over a range of spindle speeds that span an integer increase in the number of waves of vibration per tooth (e.g., $f_{tooth} = f_n$ to $2f_{tooth} = f_n$), a periodic change in the surface location will occur. This change in surface location is termed overcut when the part is smaller than commanded (i.e., more material removed than specified) and undercut when larger than commanded (see Fig. 2). This periodic variation between overcut and undercut is now described.

Consider the case of down milling with a circular tool path assumed. The normal and tangential cutting force components shown in Fig. 3 may be projected into the x and y coordinate directions using the cutter angle, ϕ, according to Eq. 3. The tangential cutting force, F_T, is taken to be proportional to the material-dependent specific force, K_S, the feed per tooth, f_t, the chip width, b, and the cutter angle. The normal (or radial) force, F_N, is assumed proportional to the tangential force. In Eq. 4, this factor is shown to be a function of β, the cutting force angle. Although the value of the cosine of this angle may vary substantially depending on the nature of the material flow at the tool-chip interface, as a first approximation 0.3 was used in these calculations [10].

$$F_x = \sum_{i=1}^{m} F_{T,i} \cos\phi_i + F_{N,i} \sin\phi, \tag{3}$$

where m = # teeth in cut at cutter angle ø,

$$F_y = \sum_{i=1}^{m} F_{T,i} \sin\phi_i - F_{N,i} \cos\phi_i$$

$$F_T = K_S b f_t \sin\phi$$

$$F_N = F_T \cos\beta, \tag{4}$$

where $\beta = 72°$ and $\cos\beta = 0.3$.

Substitution of Eq. 4 into Eq. 3 yields x and y cutting forces, each with three distinct terms: DC, sine, and cosine [4] (see Eq. 5).

$$F_x = K_S b f_t \sum_{i=1}^{m} \sin\phi_i \cos\phi_i + 0.3\sin^2\phi_i$$

$$= \frac{K_S b f_t}{2} \sum_{i=1}^{m} \sin 2\phi_i + 0.3 - 0.3\cos 2\phi_i$$

$$F_y = K_S b f_t \sum_{i=1}^{m} \sin^2\phi_i - 0.3\sin\phi_i \cos 2\phi_i \tag{5}$$

$$= \frac{K_S b f_t}{2} \sum_{i=1}^{m} 1 - \cos 2\phi_i - 0.3\sin 2\phi_i.$$

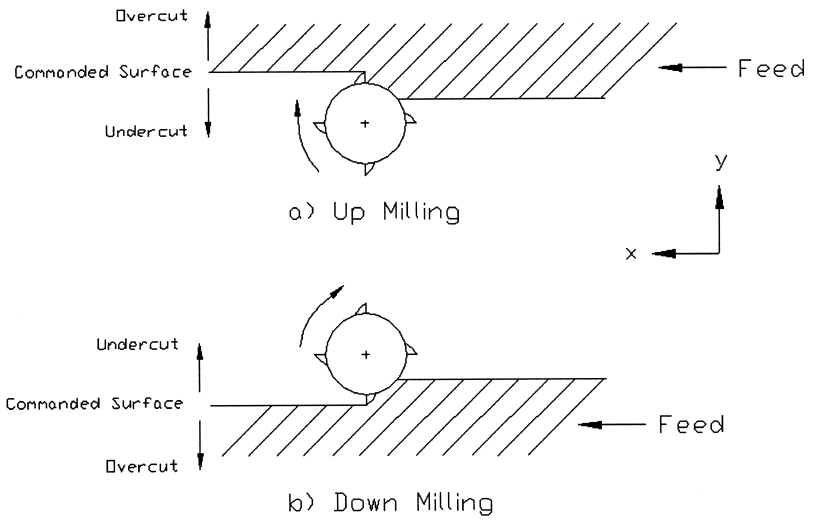

Fig. 2. Undercut/overcut in milling.

For small radial immersions, only a single tooth is in the cut at any given instant. Therefore, the cutting force is approximately constant during engagement and zero otherwise. This force is similar to an impulse with a short duration and gives strongly harmonic frequency content [7]. The frequency spectrum of the cutting force therefore includes both the fundamental tooth passing frequency and harmonics which occur at integer multiples of the fundamental frequency.

For now, consider only the fundamental frequency and its effect on the surface location error. The three term, y-force component given in Eq. 5 may be evaluated and used to find the y-deflection of the cutter (which is imprinted on the final surface at cutter angles which are odd multiples of 180° or π rad for each tooth on the cutter). The y-direction cutter displacement is phase shifted behind the y-force by an angle which is dependent on the ratio, r. Three distinct down milling cases will now be explored to explain the variation of overcut to undercut.

Case 1: $r < 1$ ($f_{tooth} < f_n$)

The three components of the y-force from Eq. 5, as well as the sum of the three components, are plotted in Fig. 4. The y-displacement which results from the two periodic (cosine and sine) force components may be found using the system transfer function ($y_i = Y/F * F_i$, $i = 1, 2$). The DC deflection is equal to the DC force divided by the static system stiffness, k. The linear magnitude and phase plots for an example single degree of freedom system are shown in Fig. 5. The magnitude and phase for a given ratio r may be calculated according to Eq. 6.

$$\frac{Y}{F} = \frac{1}{k}\frac{1}{((1-r^2)^2 + (2\xi r)^2)^{1/2}},$$

$$\gamma = -\tan^{-1}\left(\frac{2\xi r}{1-r^2}\right). \tag{6}$$

where ξ = damping ratio
k = stiffness.

It can be seen for the lightly damped system shown in

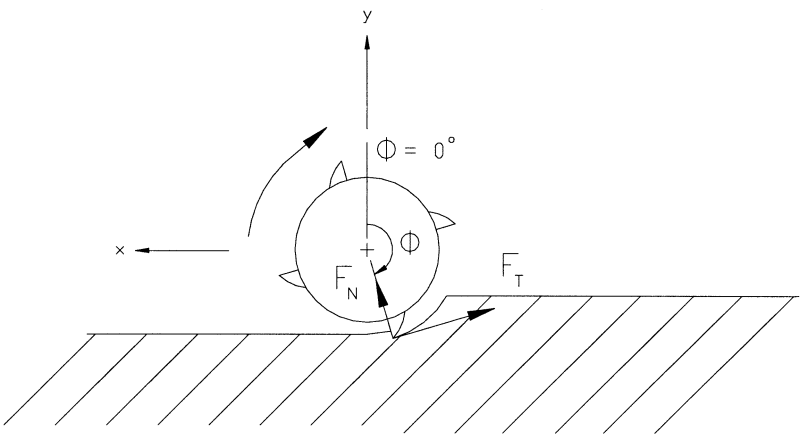

Fig. 3. Cutting Forces in Down Milling

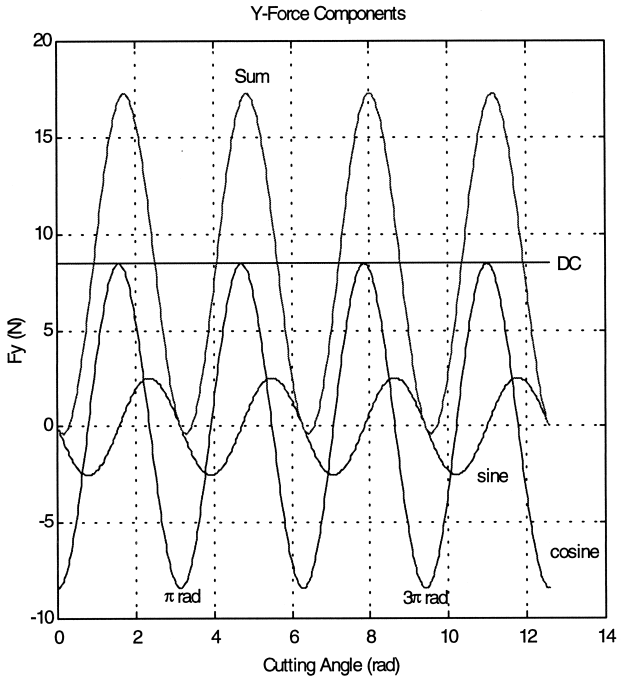

Fig. 4. Y-force components (r < 1).

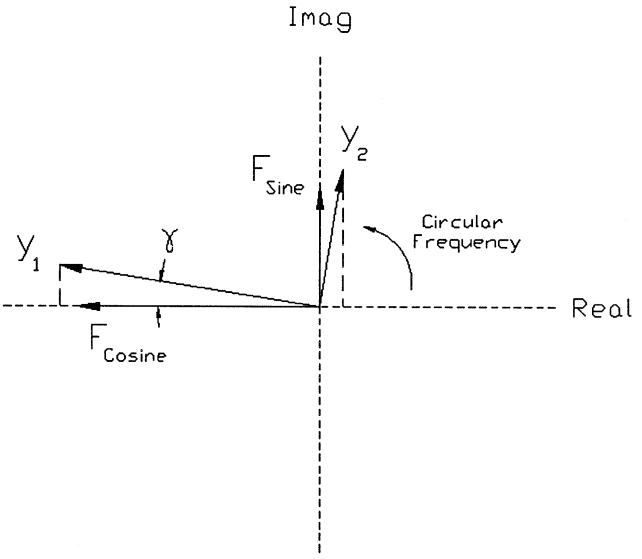

Fig. 6. Phasor diagram (r < 1).

Fig. 5 that for r < 1, the phase rapidly approaches 0° and the magnitude approaches the DC value (1/k). The two periodic components of the y-force are shown in rotating vector form in Fig. 6 at some instant when a tooth is in position 1 (from Fig. 1). The respective deflections, which lag the force by the phase angle, γ, are also shown. The cutter displacement component which results from each force term is found by projecting the phase shifted deflections onto the real axis. For the small phase lag corresponding to r < 1, the deflection due to the periodic components is dominated by the negative deflection caused by the larger cosine force component, y_1.

The three components of the y-displacement due to the three force components of Eq. 5, as well as the sum of the three components, are shown in Fig. 7, now in a time-based format and scaled using Eq. 6. The cutter angles which

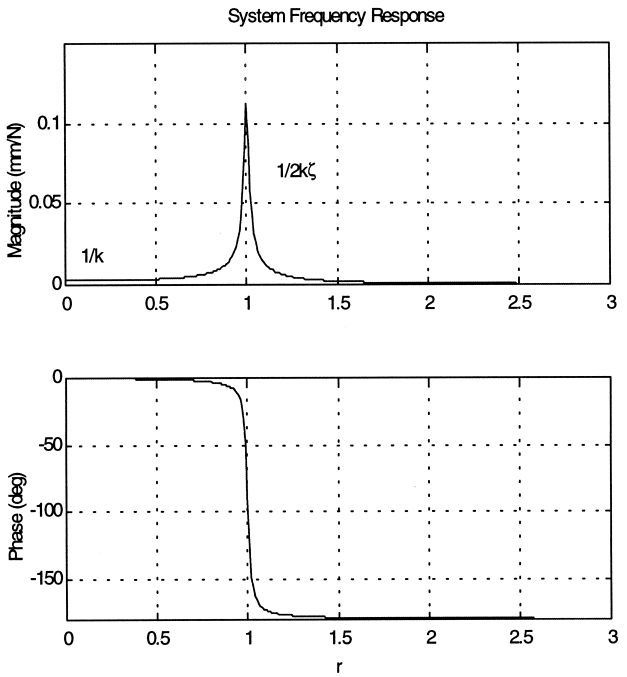

Fig. 5. System frequency response.

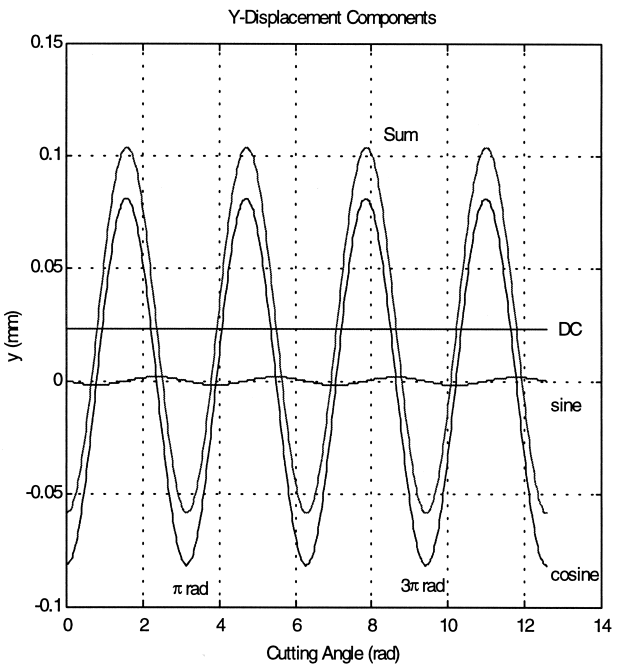

Fig. 7. Y-displacement components (r < 1).

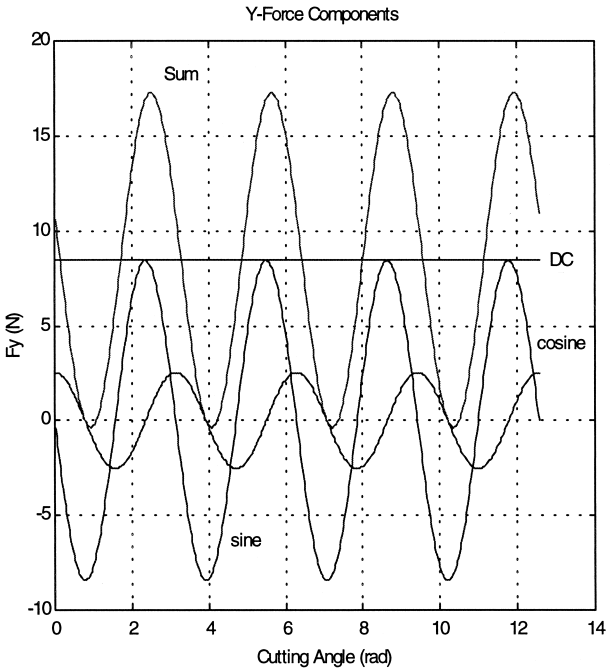

Fig. 8. Y-force components (r = 1).

produce the final surface location (odd multiples of π rad) are marked. As seen in the figure, the sum of the three deflection components is negative at the cutter locations which produce the final surface.

The final deflection may also be found by adding the real projection of the two deflection components shown in Fig. 6 to the DC deflection ($K_S b f_t/2k$). The addition of the small positive DC deflection to the large negative resultant deflection from the periodic force components produces an overcut surface since the total cutter deflection is negative (into the cut for a down milling operation).

Case 2: r = 1 ($f_{tooth} = f_n$)

As seen in Fig. 5, there is a 90° phase delay between the cutting force and deflection at resonance. Due to this phase shift, the y-force may now be re-written as shown in Eq. 7. The three force components and their sum for a single tooth including this phase shift are shown in Fig. 8.

$$F_Y = \frac{K_S b f_t}{2}(1 - \sin 2\phi + 0.3\cos 2\phi). \quad (7)$$

The corresponding deflections may again be shown in rotating vector format. In Fig. 9 it is seen that the sine force term deflection (scaled by the resonant $1/2k\xi$ factor and shifted 90° behind the force) projects no component on the real axis, while the cosine force term (scaled by the same factor and again lagging by 90°) adds a positive value to the final deflection. The final down milling surface is now assumed to be undercut since the positive deflection of the

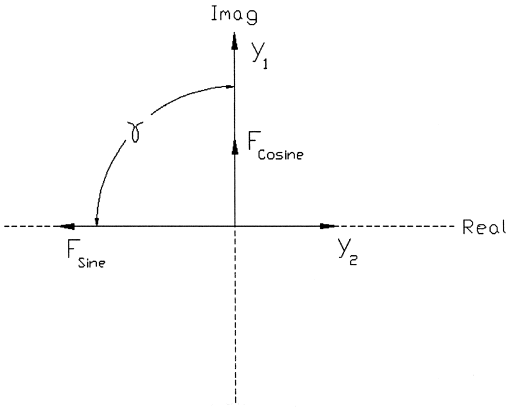

Fig. 9. Phasor diagram (r = 1).

cosine force, y_2, is added to the always positive DC deflection.

Case 3: r > 1 ($f_{tooth} < f_n$)

This situation is similar in magnitude to Case 1, but the phase now rapidly approaches -180°. The phasor diagram, shown in Fig. 10, now gives a positive deflection due to the large phase shift behind the cosine and sine terms of the y-force. When combined with the DC deflection, a final undercut surface is predicted.

The preceding examples have assumed a single fundamental component at the tooth passing frequency in the force frequency spectrum. In reality, as noted previously, this spectrum contains the fundamental tooth passing frequency as well as several harmonics of significant amplitude. For example, a reduction in spindle speed from resonance ($f_{tooth} = f_n$) to $2f_{tooth} = f_n$ causes a shift of the fundamental frequency from resonance (r = 1) to below the resonant frequency (r < 1), so a change from undercut to overcut would be expected for a down mill-

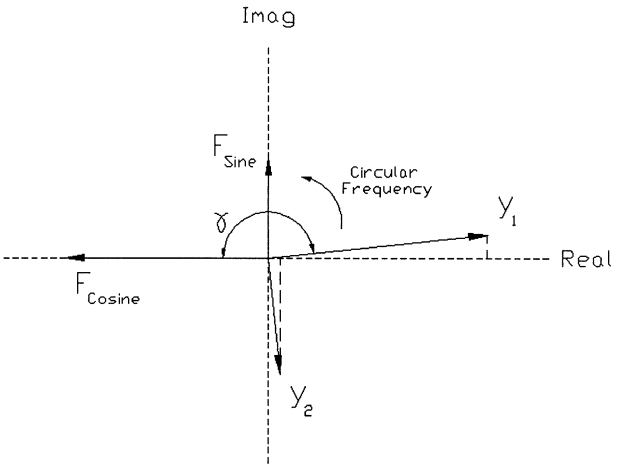

Fig. 10. Phasor diagram (r > 1).

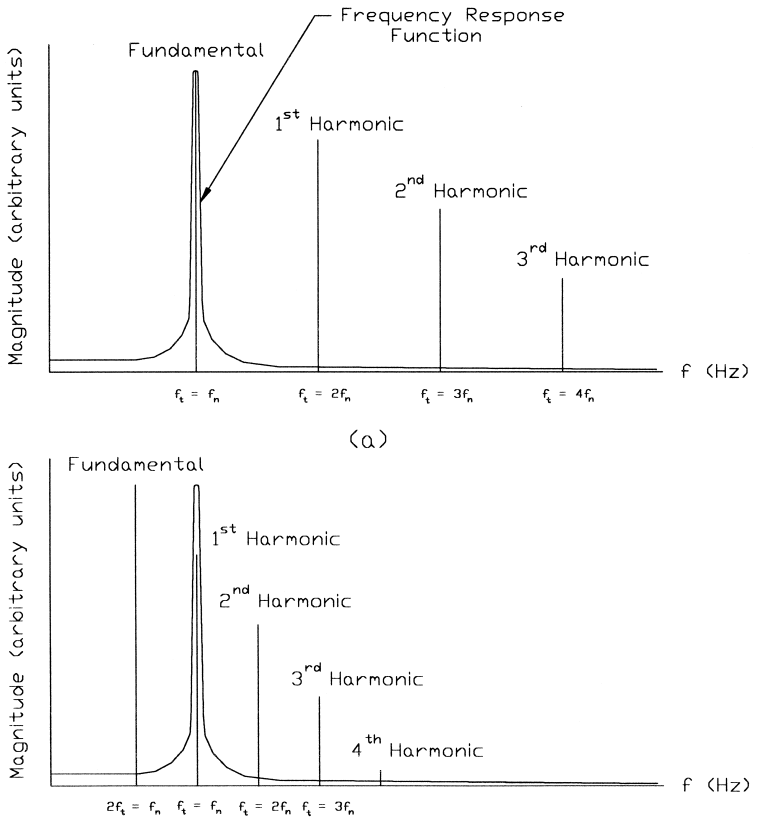

Fig. 11. Undercut/overcut/undercut transition.

ing operation. However, reducing the spindle speed to $2f_{tooth} = f_n$ also shifts the first harmonic of the fundamental frequency into the resonant position (see Fig. 11). Therefore, the situation of undercut is again seen. This periodic change from undercut to overcut and back to undercut while reducing the spindle speed is repeated until all the significant (tooth passing) harmonics are well below the system natural frequency. The situation becomes even more complex if the system has multiple closely-spaced modes of approximately equal stiffness. In this case, adjacent modes will be undergoing this periodic variation from undercut to overcut simultaneously and the surface location can be predicted only by detailed simulation.

Additionally, in the previous paragraphs, only the y-direction force and deflection (perpendicular to the final surface) were considered. In reality, for small radial immersions (e.g., finishing passes), the x-direction force grows larger than the y-direction force and the x-direction vibrations can influence the location of the final machined surface.

Another phenomenon associated with end milling cutter vibrations, defined as the profile error, is also dependent on the spindle speed, system natural frequency and stiffness, as well as the axial depth of cut [11]. For helical cutters, points on the cutting edge pass through position 1 at different instants in time along the length of the cutter. Therefore, the error of surface location described previously varies along the axial depth of cut. In this research, the axial depth of cut was kept small to avoid this particular error and isolate the surface location error only.

3. Simulation

Although the simple calculations outlined previously can reveal a picture of the cutter deflections, the final surface location error is best determined by time domain simulation. A simulation for end milling operations is described which calculates the tangential and normal forces on the cutter, the resulting cutter deflections in both the x and y-directions and the final error of surface. The simulation also includes regeneration of surface (although it is a secondary effect in forced vibrations [4]) and the non-linearity which arises when the tool jumps out of the cut due to excessive vibrations. The simulation algorithm is shown in Fig. 12.

Inputs to the simulation include the material specific force, K_s, the chip thickness or axial depth of cut, b, the feed per tooth, f_t, the spindle speed, the radial immersion and the modal stiffness, natural frequency and damping ratio of the most flexible mode in two orthogonal directions. For this elementary simulation, a circular tool path and straight cutter was assumed, which is acceptable for the low axial depths of cut used in this research. Vectors *teeth* and *phi* are

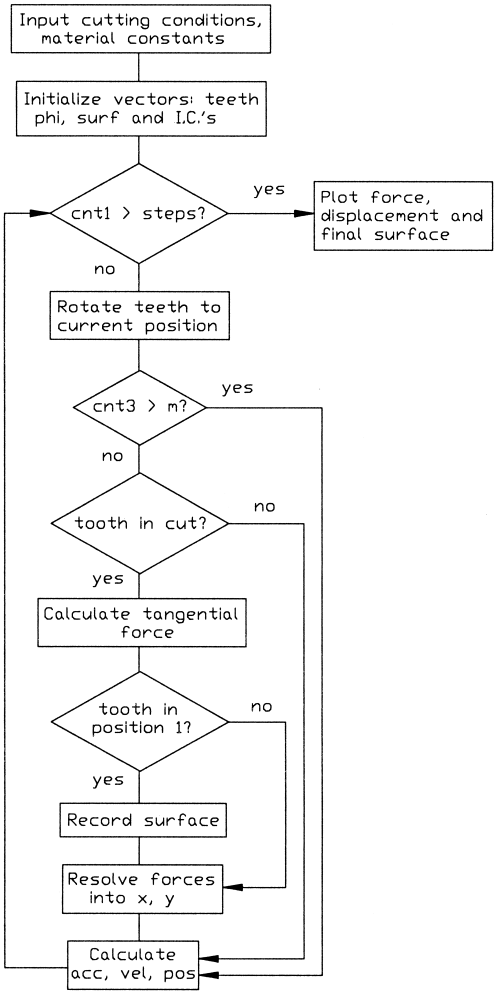

Fig. 12. Simulation flow diagram.

used to record the instantaneous teeth positions and the angle of the cutter, respectively. A vector *surf* contains the surface location left by the vibrating cutter at time steps, *dt*.

In the main body of the program, the first step is to increment the time step and index the cutter teeth to the current angular positions. The next step is to calculate the tangential force on the cutter if the current tooth is in the cut (bounded by the angles *phistart* and *phiexit*). Otherwise, it is set to zero. The tangential force is assumed proportional to the product of the material specific force and instantaneous chip load. Previous passes (recorded in the vector *surf*), the current x and y-direction vibrations of the cutter and the current feed ($f_t \sin \phi$) are used to determine the instantaneous chip load. This allows for surface regeneration. The possible non-linearity caused by a tooth jumping out of the cut during large deflections is handled by setting the magnitude of the tangential force equal to zero if a negative value for the instantaneous chip area is calculated. Next, the vector *surf* is updated and the current surface location is recorded provided a tooth is in position 1 (as shown in Fig. 1). The normal force is then calculated (see

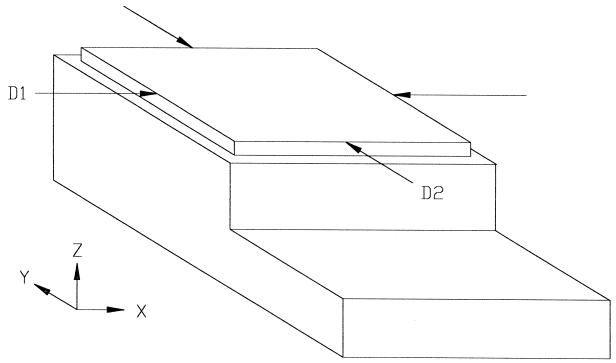

Fig. 13. Part geometry: a) X direction; b) Y direction.

Eq. 4) and the tangential and normal forces resolved into the x and y coordinate directions. This force loop is repeated for each tooth on the cutter and the forces summed. Next the cutter vibrations are calculated by Euler integration (Eq. 8) and the total loop is repeated.

$$x'' = \frac{(F_x - c_x x' - k_x x)}{m_x}$$

$$x' = x'' dt + x'$$

$$x = x + x' dt$$

$$y'' = \frac{(F_y - c_y y' - k_y y)}{m_y}$$

$$y' = y'' dt + y'$$

$$y = y + y' dt. \tag{8}$$

where c_i = damping coefficient,
m_i = modal mass.

4. Experimental method

An experimental part geometry was chosen, the CNC code written, and down milling tests completed on a horizontal spindle 3-axis CNC machining center. The workpiece (7075-T6 aluminum) dimensions were measured using a coordinate measuring machine (CMM). The part geometry is shown in Fig. 13. This particular geometry doubles the sensitivity to surface location errors because the measurements D1 and D2 each contain two passes which contribute, theoretically, the same surface error. The surface errors, E1 and E2, can then be calculated according to Eq. 9. In this equation, a positive error indicates an undercut surface, while a negative error denotes an overcut surface. The commanded values of D1 and D2 were 95.174 mm (3.747 in.) for a 12.776 mm (0.503 in.) diameter cutter.

$$E1 = (D1 - 95.174)/2,\ E2 = (D2 - 95.174)/2\ (\text{mm}) \tag{9}$$

The first step in completing the cutting tests was to find the system natural frequencies and modal values using the

impact test. A rather flexible nominally 12.7 mm (0.5 in.) diameter, 4 flute, high speed steel (HSS) helical end mill with an 82.55 mm (3.25 in.) overhang was chosen. The system direct transfer functions were obtained by attaching an accelerometer to the end of the tool, striking the tool in the direction of the accelerometer with an instrumented hammer and recording the two signals simultaneously. The fast Fourier transform (FFT) was calculated for each signal and the acceleration over force transfer function obtained by performing the complex division of the accelerometer FFT over the hammer FFT. The displacement over force transfer functions were then obtained by converting the acceleration to displacement. This conversion (dividing by $-\omega^2$ in rad/s at each point in the frequency domain) is shown in Eq. 10. The displacement over force transfer functions and the linear best fit for the x and y coordinate directions are shown in Fig. 14. These transfer functions show nearly identical tool modes in both directions with a stiffness of 3.7e5 N/m, a natural frequency of 883 Hz and a damping ratio of 0.012 (1.2%).

$$A = s^2X, \text{ where } s = j\omega, \text{ therefore, } A = -\omega^2X \tag{10}$$

Once the dominant natural frequency of the tool was known, it was possible to select the experimental spindle speeds. In the case of high-speed machining, the spindle speed selected for maximum MRR would be near the system natural frequency. For this spindle speed, there is one wave of vibration per tooth ($f_{tooth} = f_n$). The resonant spindle speed is selected by Eq. 11 with the number of waves set equal to one. The lower bound for the spindle speed could then be selected for two waves of vibration per tooth, or $2f_{tooth} = f_n$. For this range of spindle speeds, the full range between undercut and overcut would be expected for the dimensions D1 and D2.

$$\text{Spindle speed} = f_n*60/(vm) \text{ (rpm)}, \tag{11}$$

where f_n = (Hz).
v = waves per tooth
m = number of teeth on cutter

For the measured natural frequency of 883 Hz, this gives a resonant spindle speed of 13245 rpm, well within the range of today's high speed/high power spindles and the proper speed to select for maximum MRR in high-speed machining. However, the CNC machine tool available for this research had a top spindle speed of 5000 rpm. To maximize the spindle speed and cover the full range from undercut to overcut, it was decided to select an array of 11 spindle speeds between 2.65 and 3.65 waves per tooth. The chosen spindle speeds and corresponding linear feedrates for a chip load of 0.095 mm/tooth are shown in Table 1. This feed per tooth was chosen to maximize the available linear feed of 3 m/min at the top spindle speed.

This research was primarily concerned with finish machining operations when surface accuracy is of prime importance. The radial depth of cut for the cutting tests was therefore chosen to be 0.127 mm (0.005 in.), a typical finishing pass radial depth of cut in end milling operations. This corresponds to a 1% radial immersion for a nominal 12.7 mm (0.5 in.) diameter cutter. Because the purpose of

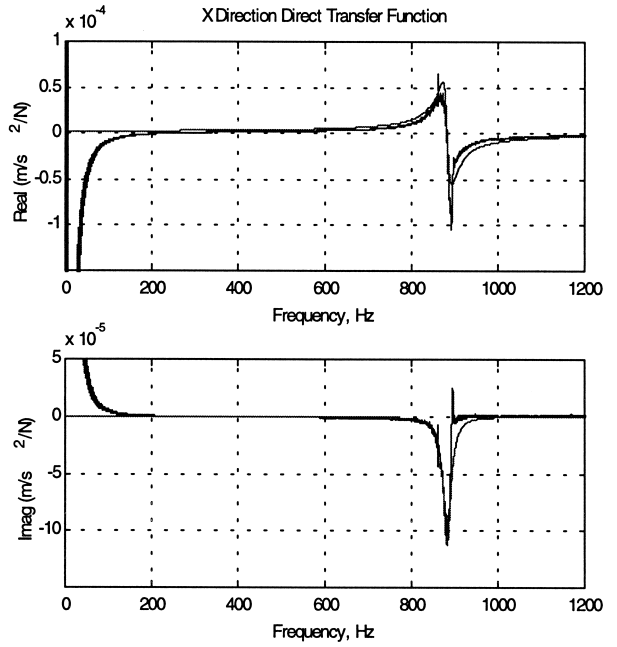

a) X Direction

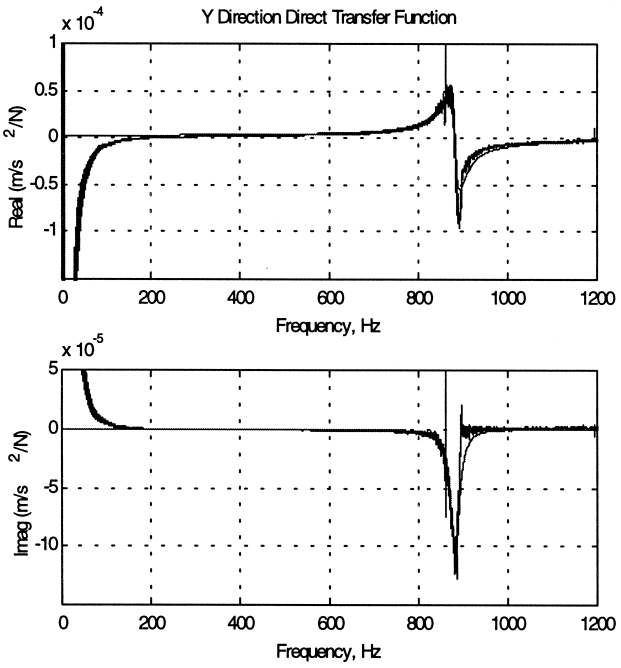

b) Y Direction

Fig. 14. Direct transfer functions for X and Y directions.

Table 1
Selected speeds/feeds

Test Number	Spindle speed (rpm)	Linear feed (m/min)
1	4998	2.95
2	4861	2.87
3	4724	2.80
4	4587	2.72
5	4450	2.64
6	4313	2.56
7	4177	2.48
8	4040	2.36
9	3903	2.28
10	3766	2.20
11	3629	2.13

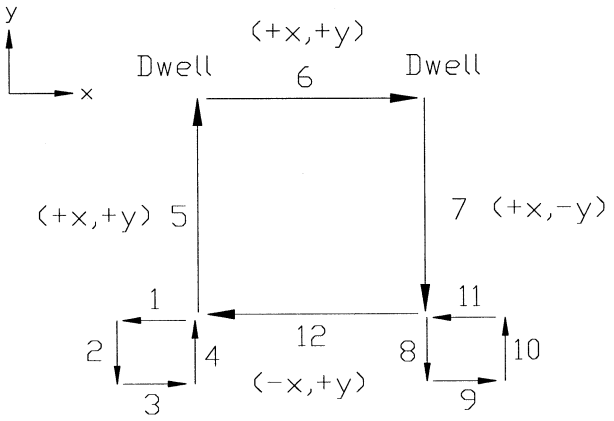

Fig. 16. NC path.

this research was to evaluate the error of surface for stable machining, it was also necessary to choose the maximum stable depth of cut for chatter-free operation at all selected spindle speeds. A commercially available software package, which produced a peak-to-peak (PTP) force diagram, was used to select this maximum allowable depth of cut [9,12]. The resultant PTP diagram is shown in Fig. 15. The PTP diagram plots the cutting force for lines of constant axial depth of cut over a selected range of spindle speeds. Abrupt discontinuities in the force along these lines signify the onset of instability, or chatter. In Fig. 15, the top line denotes an axial depth of cut of 0.50 mm (0.020 in.). Each of the lower lines represents an axial depth of cut reduced by 0.02 mm. The maximum allowable stable depth of cut over the full spindle speed range is shown to be approximately 0.28 mm. An axial depth of cut of 0.254 mm (0.010 in.) was chosen for the cutting tests.

The CNC part program used to cut the test parts was written to minimize both controller and reversal errors and, therefore, isolate the cutting force errors. For a square path with motions in only directions parallel to the machine tool axes, the dominant controller error is overshoot or undershoot in cornering operations. In an x-y corner motion, the inherent steady-state positional error, or velocity lag, allows the x motion time to decelerate and stop prior to the start of y motion. This effectively eliminates overshoot for low controller gains, but can round the corner at higher velocities. Reversal error is caused by friction in the leadscrew and produces a positional error, or dead zone, due to a force discontinuity when the direction of motion is reversed [13].

The part program chosen minimizes the effects of both these errors by dwelling for a short period before changing cutting directions and preloading the commanded axes before changing the direction of motion. Fig. 16 shows the path followed by the cutter for down-milling. The dwells, shown after moves 5 and 6, were implemented to remove the cornering dynamics and moves 1–4 and 8–11 represent the reversal preloads. The total NC program included two nested loops. The first, inner loop repeated the path shown in Fig. 16 a total of seven times with a step over of 0.127 mm (0.005 in.) in both the x and y directions between each

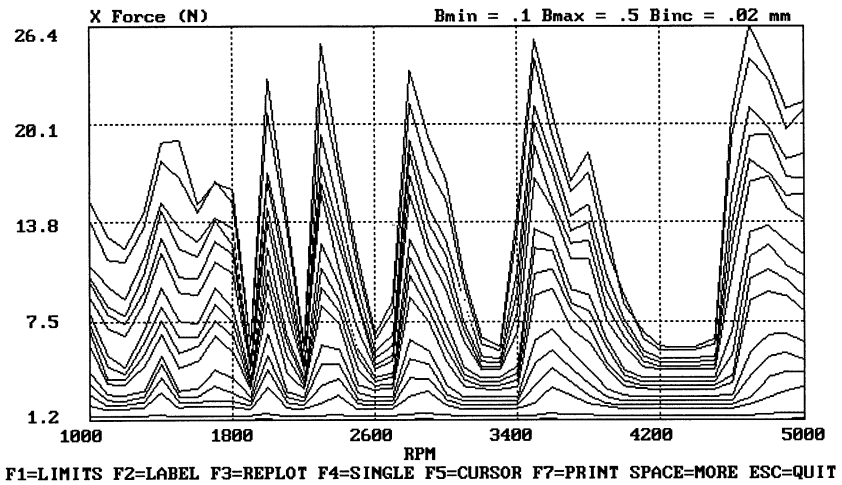

Fig. 15. PTP force diagram.

step. The second, outer loop repeated the inner loop 12 times while increasing the axial depth of cut in the z direction by 0.254 mm (0.010 in.) each repetition.

Another potential source of error is asynchronous error motions of the machine tool spindle and structure. If the asynchronous errors were larger than the surface location error due to cutter vibration, the cutting tests described previously could yield seemingly random results. The results would still be deterministic, however, since the spindle motions would, in this case, mask the cutting errors and produce the seemingly random results. Therefore, the 'grease pencil test' or single spot asynchronous motion test, a common procedure used to measure these error motions, was completed on the spindle to be used in the cutting tests [14]. In the grease pencil test, a rotating reference surface (such as a workpiece, chuck, or the spindle nose) is selected. A displacement transducer, such as a capacitance probe, is then mounted perpendicular to the reference surface and fixed to ground. A high or low point (e.g., the mark left by a grease pencil) disrupts the dielectric between the probe and measurement surface once per revolution. For a perfect spindle, the capacitance voltage would be the same for each revolution. In reality, the maximum change in the peak voltage over several revolutions represents the asynchronous error at a specific angular location.

Care must be taken in digitally recording the data to prevent aliasing. The sampling rate must be at least twice the highest expected frequency (or twice the bandwidth of the displacement indicator). For these tests, a 15.011 kHz sampling rate yielded an approximate radial asynchronous error motion of 1.78 μm (0.070e-3 in.). The digital record of the calibrated capacitance output is shown in Fig. 17. In this case, the asynchronous error magnitude is much smaller than the expected error due to cutter vibrations and may be neglected. However, in other situations, as noted previously, this error could completely conceal the cutting force errors.

Once the part was machined at a given spindle speed, it was removed from the machine and placed in a thermally stable environment (68° $\pm$ 0.2° F) to soak overnight. The following day, a direct computer-control part program was executed on the CMM to measure the 2-D distances D1 and D2. The program first allowed the user to align the CMM local measurement axes with those of the part, then probed five points along each of the edges of the part to determine D1 and D2 using a 2 mm diameter probe. Direct computer-control allows the CMM controller to select the normal to the probing surface and approach each measurement point with a constant velocity. This effectively reduces the uncertainty of the measurements. Additionally, the CMM measurement program was executed sequentially 12 times. The high and low values were rejected and the other 10 averaged. A standard deviation of less than 1 μm was typical.

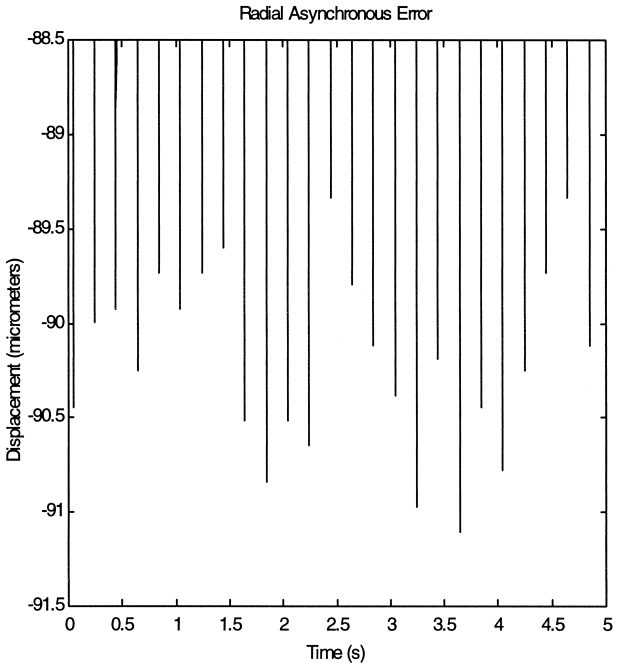

Fig. 17. Radial asynchronous error.

5. Experimental results

The machining and measurement of 11 total parts corresponding to the spindle speeds/feeds shown in Table 1 were completed. The error of surface location was then calculated according to Eq. 9. Additionally, the simulation previously described was executed for the same speeds/feeds to find the predicted error of surface location. A comparison of the experimental and simulated results for both the D1 and D2 surfaces is shown in Fig. 18

It can be seen from Fig. 18 that the simulation results match well with the experimental data at speeds of 4313 rpm and above. The predicted overcut to undercut can be seen in both the simulated and D1 surface data with the maximum undercut at 4450 rpm (near the second harmonic

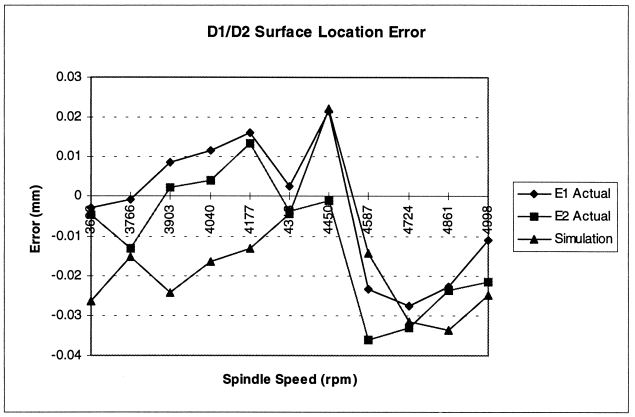

Fig. 18. D1/D2 Surface location error.

of resonance). The D2 surface data shows a probable anomaly at the 4450 rpm spindle speed, but good agreement with the D1 data otherwise. The good experimental agreement between the two surface errors is reassuring since the x- and y-direction system dynamics were equal, so the errors should be the same. The discrepancy between the simulated and experimental results at spindle speeds below 4313 rpm (which appears to be a simple offset except at 3766 rpm) could have resulted from several procedural limitations. First, only one part was machined at each spindle speed so the process uncertainty is unknown. Second, only one part was machined per day over an 11-day period (to allow an overnight thermal soak of the workpiece before measurement). The total shop temperature variation for the machining environment was significant over this time period, but the measuring environment was kept at a constant temperature of 68° F. (In each case, however, test parts were produced from a "cold" machine state and the light finishing passes introduced little heat into the test part during machining.) Finally, the end mill was removed after each test, so the part could be faced with a separate tool (to limit wear). Therefore, the positioning repeatability of the spindle collet becomes a factor.

Although the simulation and experimental results do not match perfectly, a large variation in the surface location error is recognized, as well as agreement in the error trends, over the range of spindle speeds tested in both data sets. A total experimental variation in surface location error of 50 μm (0.002 in.) is shown over the range of spindle speeds for the surfaces under identical cutting conditions using the same NC program. In certain finish machining applications, this is an unacceptable error magnitude. It can also be seen that at spindle speeds of 3770 and 4520 rpm for D1 and 3890 and 4300 rpm for D2 there is no error. Selection of these speeds would produce a part with no error of surface introduced by the cutting operation, even for this flexible tool.

To see the effect of spindle speed over a larger range, simulations were executed using the same cutting conditions, tool dynamics, and an assumed spindle speed range of 1000–15000 rpm. These results are shown in Fig. 19. The periodic variation of overcut to undercut can be seen in the figure. The forcing function harmonics are also marked (i.e., "2" represents the second harmonic where $3f_{tooth} = f_n$). It is important to note the magnitude of change in surface location possible by a simple change in spindle speed. For a change in spindle speed from 1950 to 6623 rpm, for example, a change in surface location error of 70 μm (0.0028 in.) is predicted. This result may be equal to or bigger than the effect of typical individual error sources (i.e., geometric and thermal errors). Perhaps more importantly, it can be seen in Fig. 19 that at tooth passing frequencies near harmonics of the system natural frequency, a small change in spindle speed results in a large change in surface location error. For example, a change in spindle speed from 6623 (first harmonic) to 7200 rpm will cause a change in surface location

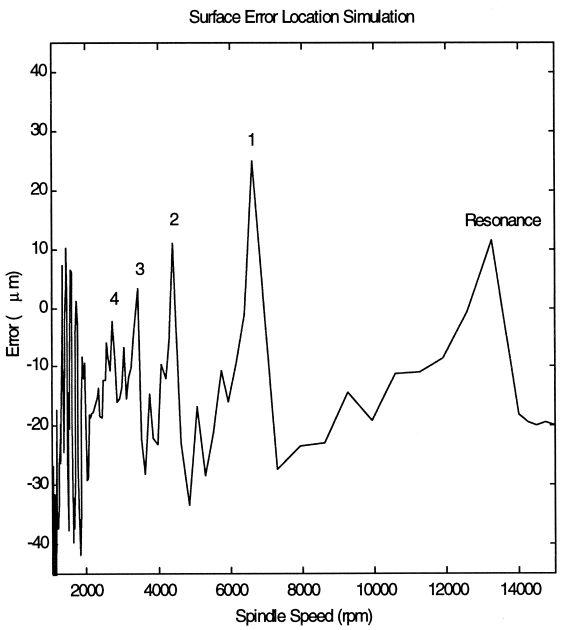

Fig. 19. Full range simulation (0.5 in. diameter tool, 3.25 in. overhang).

error of 53 μm. Both speeds provide stable cutting conditions. However, due to a change in the phasing of the cutter vibrations, the surface location varies significantly.

As noted, the cutting tool used in this research was quite flexible. In other situations, a less flexible tool, with a different frequency response function, might be used. As an example, consider a 4 flute, 19.05 mm (0.75 in.) diameter, helical HSS end mill with a 38.1 mm (1.5 in.) overhang and a higher natural frequency than the previous tool (1200 Hz), approximately three times the stiffness (1e6 N/m) and 1% damping in both the x and y directions. The simulations shown in Fig. 20 were once again executed, but with these new modal values for the machine/tool system. The results are shown in Fig. 20. Once again, the periodic undercut/overcut variation can be seen, but now at different harmonic frequencies. It can also be seen that the overall magnitude of undercut to overcut is now smaller due to the less flexible tool.

6. Conclusions

The effect of spindle speed and the system frequency response function on the surface location error in finish machining has been explored. Cutting tests have been performed over a range of spindle speeds corresponding to a full range of surface location errors from overcut to undercut ($2.65f_{tooth} = f_n$ to $3.65f_{tooth} = f_n$) for a given tool and stable cutting conditions. Simulations have also been completed and good agreement found between the simulated and actual data over a limited spindle speed range. Further cutting tests, which include several tools and various materials and cutting conditions, will be necessary to fully ex-

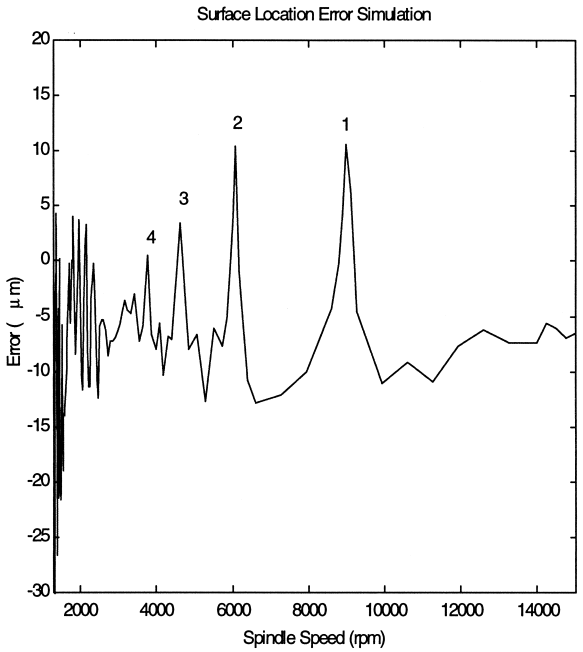

Fig. 20. Full range simulation (0.75 in. diameter tool, 1.5 in. overhang).

plore this phenomenon. Although not a definitive work, this research demonstrates a significant dependence of the surface location error on spindle speed. Furthermore, it has been observed that a relatively small change in spindle speed can produce a large variation in the final surface location (and part dimensions), especially at speeds near integer fractions of the system natural frequency. This research shows that both system natural frequency and flexibility are important considerations, especially in high-speed machining where the tooth passing frequency is set near the natural frequency (resonance) to maximize the stable depth of cut.

Although this research concentrated on the surface location error due to cutter vibrations, this is only one error source within the machining process. Other sources, such as geometric, thermal, or hysteresis errors, may dominate in a given situation. For example, in the machining center used in this research, a large reversal error (32 μm) was present in the x-axis while virtually no reversal error occurred for the y-axis (controller compensation was turned off for the experiments). If the NC path included an x-direction reversal without a corresponding preload to remove this error, the x reversal error would have increased the D1 surface dimension by 32 μm. Additionally, for a nonsymmetric part, thermal growth of the spindle in the radial direction would affect the part's final dimensions. Finally, although the dynamics of the cutting process have been modeled and tested, material removal also introduces heat into the system. Therefore, thermal effects are not easily decoupled from the cutting process. In short, all errors in the machine tool, including the dynamic cutting errors, must be accounted for and compensated if highly accurate parts are to be manufactured.

Acknowledgments

This work was supported in part by the National Science Foundation under grant numbers DDM-935138 and DGE-9354980.

References

[1] Hocken R. Machine Tool Metrology, Tutorial at the American Society for Precision Engineering 9th Annual Meeting, Cincinnati, OH, October, 1994.
[2] Blaedel KL. Error reduction. In: Technology of Machine Tools, Vol. 5: Machine Tool Accuracy. Livermore, CA: University of California, UCRL-52960-6, October 1980.
[3] Software Correction of Precision Machines. A Report from the Precision Engineering Laboratory at UNC Charlotte to the National Institute of Standards and Technology, NIST-60NANB2D1214, July, 1993.
[4] Tlusty J. Class Notes EML 6934: Fundamentals of Production Engineering Part 2. University of Florida, Fall Semester, 1994.
[5] Smith S. Chatter, Forced Vibrations, and Accuracy in High Speed Milling. M.S. Thesis, University of Florida, 1985.
[6] Altintas Y, Budak E. Analytical prediction of stability lobes in milling. Annals of CIRP 1995;44-1:351–62.
[7] Chau W. Accuracy of Milling Operations Based on Dynamic Models and Simulations. M.S. Thesis, University of Florida, 1992.
[8] Smith S, Tlusty J. Update on high-speed milling dynamics. ASME Journal of Engineering for Industry 1987;112:142–9.
[9] Smith S, Tlusty J. Current trends in high speed machining. Journal of Manufacturing Science and Engineering 1997:119:664–6.
[10] Tlusty J. Class Notes EML 6934: Fundamentals of Production Engineering Part 1, University of Florida, Fall Semester, 1994.
[11] Tlusty J. Cutting Tests: Report Presented to the ASME B5 Committee. 1990 ASME B5 Committee Meeting, January, 15, 1990, pp. 8–9.
[12] User's Manual: MILSIM Version 2.0. Gainesville, FL: Manufacturing Laboratories, Inc., 1992.
[13] Slocum A. Precision Machine Design. Englewood Cliffs, NJ: Prentice Hall, 1992.
[14] Draft Revision of ASME/ANSI B89.3.4: Dimensional Metrology - Axes of Rotation Standard. February, 1998.